Representing dynamic urban land change in the Community Earth System Model (CESM)

Bowen Fang[1], Lei Zhao[1,2,3,*], Keith Oleson[4,*], Keer Zhang[5], Peter Lawrence[4], Bill Sacks[4], Chang Cao[6,7], Chunyang He[8,9], Qingxu Huang[8,9], Zhifeng Liu[8,9], Xuhui Lee[5]

[1] Department of Civil and Environmental Engineering, University of Illinois at Urbana-Champaign, Urbana, IL, USA.

[2] Institute for Sustainability, Energy, and Environment (iSEE), University of Illinois at Urbana-Champaign, Urbana, IL, USA.

[3] National Center for Supercomputing Applications, University of Illinois at Urbana-Champaign, Urbana, IL, USA

[4] Climate and Global Dynamics Laboratory, National Center for Atmospheric Research, Boulder, CO, USA.

[5] School of the Environment, Yale University, New Haven, CT, USA

[6] Center on Atmospheric Environment, International Joint Laboratory on Climate and Environment Change (ILCEC), Nanjing University of Information Science and Technology, Nanjing, China

[7] Key Laboratory of Meteorological Disaster, Ministry of Education and Collaborative Innovation Center on Forecast and Evaluation of Meteorological Disasters, Nanjing University of Information Science and Technology, Nanjing, China

[8] Center for Human-Environment System Sustainability (CHESS), State Key Laboratory of Earth Surface Processes and Resource Ecology (ESPRE), Beijing Normal University, Beijing, China

[9] School of Natural Resources, Faculty of Geographical Science, Beijing Normal University, Beijing, China

* Correspondence to: Lei Zhao (leizhao@illinois.edu) and Keith Oleson (oleson@ucar.edu)

Abstract:

Urbanization (urban land change) alters local and regional climate through biophysical and biogeochemical processes and has broader climate impacts through atmospheric feedbacks. Despite its critical climate impacts, urban areas have rarely been explicitly represented in global-scale Earth system models, and physically-based transient urban representations are missing as well. The Community Earth System Model (CESM) has a physically based urban land parameterization – Community Land Model Urban (CLMU) – that is sufficiently detailed to represent the properties and processes in the urban environment. We improve this model by implementing a dynamic urban scheme to represent transient land use due to urbanization. Leveraging existing urbanization projection datasets, the new scheme allows urban extent to be updated annually during a climate simulation while conserving energy and mass balance during the transition. Land-only simulation results confirm the robustness of the new dynamic urban scheme and demonstrate the direct local climate effects induced by urban land expansion. In the appendix of this paper, we also document two recent improvements to the building energy scheme of CLMU.

Plain Language Summary

The Community Land Model Urban (CLMU) is the urban component of the Community Earth System Model (CESM) for simulating the urban effects on local climate on the global scale. Although CLMU features a realistic physical representation of cities, a key limitation is that its urban extent does not change over time, even if urban land change is and will continue occurring in reality due to rapid urbanization. This paper describes a new transient urban capability in CLMU where urban extent in the model can change dynamically throughout a simulation, thus

61 further enhancing the accuracy of the urban representation. We demonstrate the difference in
62 local urban climate when the urban area is changed annually according to a projection, compared
63 to when urban extent stays unchanged. This new model capability provides an essential modeling
64 infrastructure to investigate the combined effects of future global climate change and
65 urbanization on local urban climates. In the appendix we also present two improvements to the
66 CLMU that improve the accuracy of building energy simulation.
67
68
69
70
71 **Key points**

72 1. A new transient-urban capability for CESM enabling dynamic urban representation
73 consistent with climate change scenarios is developed.
74 2. Urban land time series datasets are developed and model tools are modified to allow for
75 user-supplied urban projection for CESM simulations.
76 3. Simulations with the new transient urban feature demonstrates local climate effects
77 caused by urbanization coupled with climate change.
78
79
80
81
82

1. Introduction

Cities are hotspots of climate change hazards, exposure, and vulnerability (Grimm et al., 2008; IPCC, 2014; Mora et al., 2017; Tuholske et al., 2021; J. Yang et al., 2023; Zhao et al., 2021a). Global climate change is projected to elevate both persistent stress (such as prolonged heat stress and water scarcity) (Gray et al., 2023; He et al., 2021; IPCC, 2021; Knutti & Sedlacek, 2013; J. Li et al., 2018; Patz et al., 2005) and the intensity, frequency, and duration of climate extremes (such as heatwaves, extreme rainfall, flooding, and droughts) (Fischer et al., 2021; Horton et al., 2016; Meehl & Tebaldi, 2004; Pal & Eltahir, 2016; Zheng et al., 2021; Zscheischler et al., 2018). Urbanization modifies the land cover and alters local and regional weather and climate through biophysical and biogeochemical processes (Manoli et al., 2019; Niyogi et al., 2011; Qian et al., 2022; B. Yang et al., 2019; Zhao et al., 2014), further amplifying those climate-driven hazards (Baklanov et al., 2018; Cao et al., 2016; D. Li & Bou-Zeid, 2013; Zhao et al., 2018). Over half of the world's population currently lives in urban areas, and because of rapid urbanization, this will exceed 68% by the middle of this century (UNDESA, 2018). The concentrated population as well as civil infrastructures (such as energy, water, and transportation infrastructures) put cities among the most exposed societal sectors to climate threats (Lai et al., 2022; Lai & Dzombak, 2021; Tuholske et al., 2021; J. Yang et al., 2023). In addition, cities are a mix of socioeconomic and demographic groups. The disadvantaged communities with limited resources for services, hospitality, and utilities are disproportionately vulnerable to climate hazards (Chakraborty et al., 2019; Hsu et al., 2021; Kaur & Pandey, 2021; Y. Li et al., 2018; Salami et al., 2017; Ye et al., 2021). These risks – intersection of climate hazards, exposure, and vulnerability (IPCC, 2022) – will likely increase in the future under rapid urbanization coupled with climate change (Huang et al., 2021; Krayenhoff et al., 2018; Luo & Lau, 2018, 2019; Zhao, 2018). There is a pressing need

106 to understand future urban-specific climate change, dynamics, and the associated risks to inform
107 effective urban mitigation and adaptation strategies (Krayenhoff et al., 2021; Zhao et al., 2017a).
108
109 Despite the critical importance of urban climate impacts, nearly all Earth system models (ESMs)
110 lack an explicit representation of urban areas compared to natural vegetated or rural surfaces
111 (Hertwig et al., 2021; Masson, 2006; Zhao et al., 2021b). The omission of physical-based urban
112 representation across ESMs stems from early versions of global climate models designed for
113 large-scale dynamics in which urban areas were too small to cause discernible effects. This
114 shortcoming hinders not only the simulation of urban effects on local to regional climates, but
115 also the model development addressing coupled human-Earth systems.
116
117 The Community Earth System Model (CESM, Danabasoglu et al., 2020) is one of the very few
118 ESMs participating in the Coupled Model Intercomparison Project (CMIP) (Eyring et al., 2016;
119 Taylor et al., 2012) that has a physically based urban representation (Lawrence et al., 2019;
120 Oleson et al., 2008). In CESM, urban surfaces and their interaction with the lower atmosphere
121 are represented in the Community Land Model Urban (CLMU) based on the urban canyon
122 concept (Oleson & Feddema, 2020). As an explicit urban representation embedded in CESM,
123 CLMU has been extensively evaluated against ground-based and remote sensing observations
124 over cities across the globe (Cao et al., 2016; Demuzere et al., 2008, 2013, 2017; Fischer et al.,
125 2012; Fitria et al., 2019; Jackson et al., 2010; Karsisto et al., 2016; Oleson, 2012; Oleson et al.,
126 2008; Zhao et al., 2014, 2017). Several other ESM model groups have recently begun to
127 incorporate an urban representation in their models. For example, the Geophysical Fluid
128 Dynamics Laboratory (GFDL)'s land model (LM3) deploys an urban canopy model (LM3-UCM)

129 to simulate energy, water and carbon exchange between land and atmosphere in urban regions (D.
130 Li et al., 2016a, 2016b).

131

132 Even for ESMs that have an urban representation, a critical limitation is that they lack the
133 transient urban capability, that is, the ability to represent changes in urban extent in time during a
134 transient climate simulation. Although dramatic changes in urban extent are expected in the
135 future (Bren d'Amour et al., 2017; Seto et al., 2017; William Solecki et al., 2013), these changes
136 and their effects have not previously been represented in transient climate simulations. We note
137 that LM3-UCM has an option to set an annual rate at which other landscape transitions into
138 urban, but this transition is uniform globally and cannot provide the essential geospatial
139 granularity (D. Li et al., 2016a). This universal lack of a transient urban scheme implies that,
140 while the anthropogenic greenhouse gas (GHG) emissions that urban land makes a significant
141 contribution to (Creutzig et al., 2015; Seto et al., 2014) are normally prescribed in future
142 simulations as climate change scenarios (O'Neill et al., 2016; Taylor et al., 2012), the urban land
143 cover is not consistent with those scenarios. This creates a critical technical barrier for existing
144 models to simulate the dynamic interactions between the changing and emerging urban land
145 patterns and climate systems, specifically, the urban development effects on the radiative, heat,
146 mass, and momentum fluxes and as a result on the local and regional environments. We argue
147 that representing urban landcover dynamically is essential for global urban climate modeling.

148

149 Here our work fills this critical modeling gap by implementing a dynamic urban scheme into the
150 CESM, making it the first ESM to incorporate transient urban land. The new scheme will expand
151 CESM's capability in urban modeling through more flexible urbanization representation. This

work leverages recent advances in CLM development (Lawrence et al., 2019; Oleson & Feddema, 2020) and urban land projection data. We have compiled two urbanization datasets based on datasets developed by Beijing Normal University (BNU) (He et al., 2021) and Gao and O'Neil (2020) that we test in our new scheme. Although only future projected transient urban land use is demonstrated in this paper, the methods outlined here can easily incorporate historical transient urban land datasets when the data becomes available. In addition, we have expanded the capability of an existing Community Terrestrial Systems Model (CTSM) tool that enables users to supply other urbanization projections for CESM simulations. CTSM is CESM's land sub-model and includes previous versions of the land model such as CLM5 (Lawrence et al., 2019). The new dynamic urban scheme will be included in the next CTSM release (CTSM5.2), which will become the land model component for CESM3.

This paper documents the implementation of the dynamic urban scheme in CESM version 2 (CESM2). Section 2 provides an overview of CESM, its land component – CTSM, and the urban parameterization (CLMU). The development of the dynamic urban scheme is introduced in Section 3, along with the datasets and tools used to produce surface datasets for dynamic urban simulation. A land-only simulation with the dynamic urban scheme and its results are described in Section 4. In the Appendix, we also document recent improvements in the building energy scheme of CLMU that are now available in CTSM.

2. Urban modeling in CESM

2.1 Brief overview of CESM, CTSM and CLMU

CESM is a fully coupled Earth system model consisting of sub-model components resolving properties and processes for land, atmosphere, ocean, sea ice, land ice, river, and wave. These components are linked through a coupler to exchange fluxes (Danabasoglu et al., 2020). Among these components, the CTSM is the land model that represents terrestrial ecosystems' mass and energy cycling processes and their contributions and responses to climate variability. CTSM characterizes Earth's heterogeneity through a nested hierarchy (Figure 1A), where each grid cell can have up to seven land units including three urban density types (tall building district, high density, and medium density) and vegetated, crop, glacier, and lake land units. Each land unit is further divided into columns (e.g., the urban land units consist of roof, sunlit and shaded wall, and pervious and impervious canyon floor) and then patches (e.g., plant functional types). Such hierarchy captures the biogeophysical and biogeochemical processes specific to each land use and land cover type. In each grid cell, land units are driven by the common climate forcings and interact with other model components through the coupler simulating the terrestrial ecosystem's interactions with the climate system.

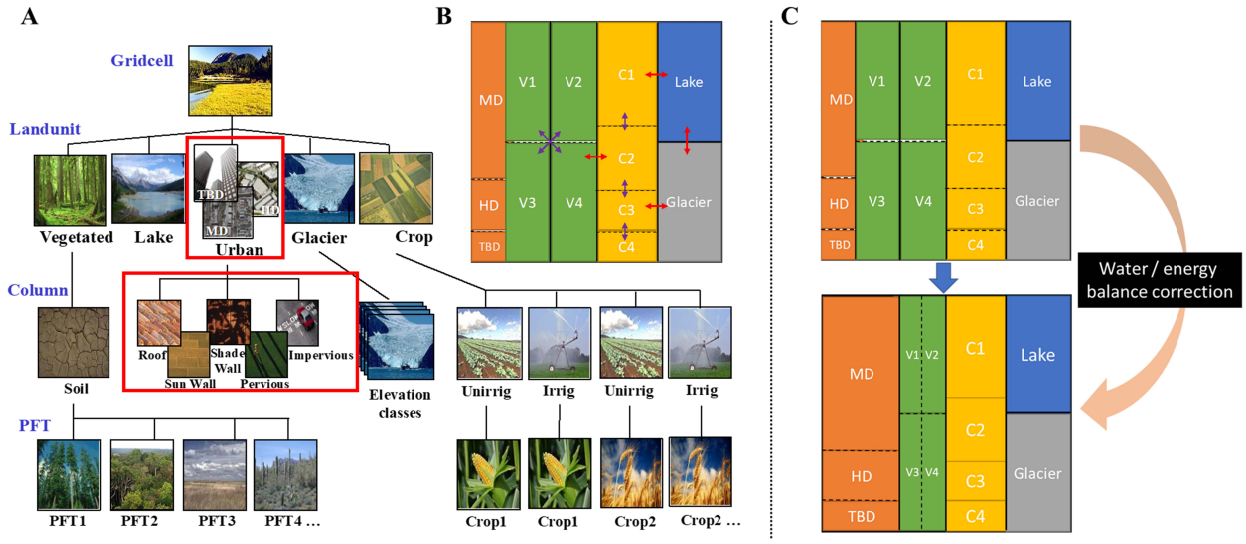

Figure 1. CESM representation of land heterogeneity and transient land use land cover change. ***A:*** *CESM's nested hierarchy that represents land heterogeneity. Urban: TBD = tall building district; HD = high density; MD = medium density. Vegetated – PFT: plant function type. Crop – Unirrig: unirrigated. Irrig: irrigated.* ***B:*** *Box shows hypothetical sub-grid distribution for a single grid cell. Vegetation: V1 to V4 denote different plant function types. Crop: C1 to C4 denote different crops or management behaviors (rainfed or irrigated). Red arrows indicate allowed land unit transitions. Purple arrows indicate allowed lower-level transitions. In this existing infrastructure, urban land is not allowed to change.* ***C:*** *The dynamic urban scheme. Urban expansion here is represented by increasing the urban land units' fractional area in the grid cell. Due to the increase in urban fraction, the grid cell total water and energy content is altered, which is accounted for by dynamic balance fluxes for water (liquid and ice runoff to/from river) and heat (sensible heat flux to/from atmosphere), shown as "Water/energy balance correction".*

The urban land unit and its interaction with the lower atmosphere are represented in the Community Land Model Urban (CLMU) as part of CTSM. This urban representation is based on an urban canyon concept which divides each urban land unit into five facets or columns: roof, sunlit wall, shaded wall, and pervious and impervious surfaces on the canyon floor (Figure 2). The urban representation accounts for the surface energy balance (radiation trapping, thermal conduction, air conditioning and heating), hydrology (roof and canyon floor snowpack, water ponding and run-off, and evaporation), and exchange of heat, moisture, and momentum with the atmosphere for each individual facet (Oleson et al., 2008). An existing global urban surface dataset is embedded in the model (Jackson et al., 2010, hereinafter **J2010**). This dataset

prescribes the present-day (circa-2000) urban extent, and thermal, radiative, and morphological properties for every grid cell having an "urban" subgrid land unit. CLMU is simple enough to operate within a global-scale Earth system model yet sufficiently realistic and detailed to simulate the urban surface biophysical and hydrologic processes and to capture urban effects on surface climate across scales.

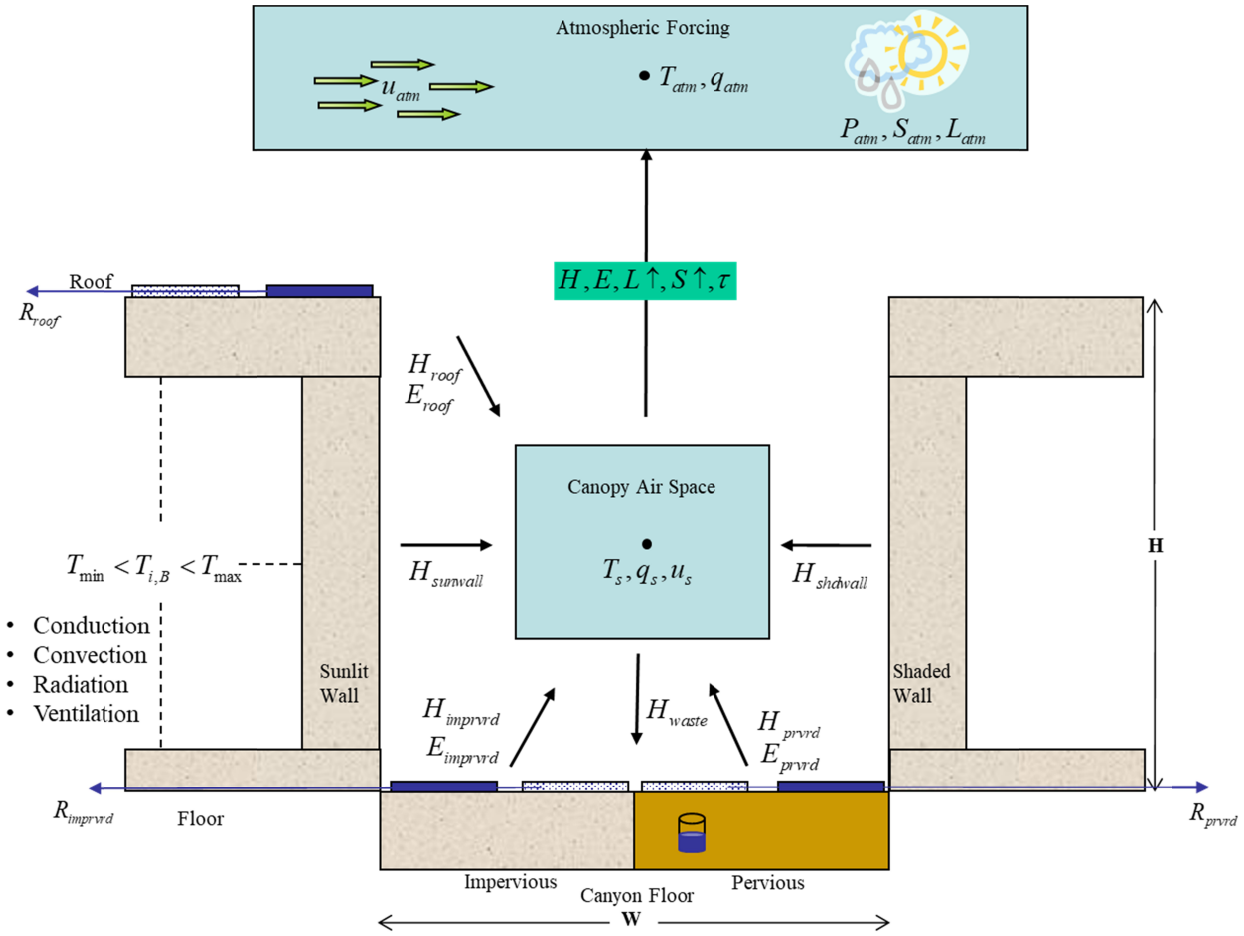

Figure 2. Schematic diagram of CLMU's urban representation, based on a conceptual urban canyon model (Adapted from Oleson & Feddema, 2020).

2.2 Recent advances in CLMU

After the initial release of CLMU (Oleson et al., 2008) as part of Community Land Model version 4 (CLM4), there have been multiple updates to the urban model that continue to enhance its capabilities (Oleson & Feddema, 2020). First, instead of simulating only one urban land unit per grid cell, multiple urban density classes are introduced, partitioning the urban tile into three density types: tall building district (TBD), high density (HD) and medium density (MD), and each density class demonstrates distinct physical properties. This feature takes full advantage of the existing urban surface dataset (J2010) and provides more granularity for a realistic urban representation than the original version. Second, an urban properties tool was developed to create future urban development scenarios more easily. Third, the CLMU's building energy model (BEM) was modified to improve its performance in modeling anthropogenic heat fluxes associated with space heating and air conditioning. Lastly, CLMU is now able to generate various heat stress indices that describe the comfort level of urban residents. Details of these model advances are documented in Oleson & Feddema (2020). Two additional updates have been made to the BEM since that time. Building width in the BEM is now explicitly derived from data in J2010 instead of being assumed to be equal to street width. Second, the ventilation flux from building interior to urban canopy air was not being accounted for, and this has now been remedied. Details about these updates, including results from a simulation designed to test the impact on urban canopy air temperature and anthropogenic heat fluxes, can be found in the Appendix.

3. Implementation of dynamic urban capability

The current urban representation in CLMU is static, which means that the urban extent and property data initialized at the start of a simulation are time-invariant throughout the simulation

(**Figure 3A**). This is in contrast with the treatment of other land units in CESM. Percent cover of natural vegetation, cropland, and glaciers can be adjusted throughout the course of a simulation, referred to here as transient land use (Figure 1B). The transient land use is implemented through two major mechanisms: (i) via a land use dataset (Hurtt et al., 2020) prescribing the land use conversion, or (ii) through prognosed initiation or loss of glacier.

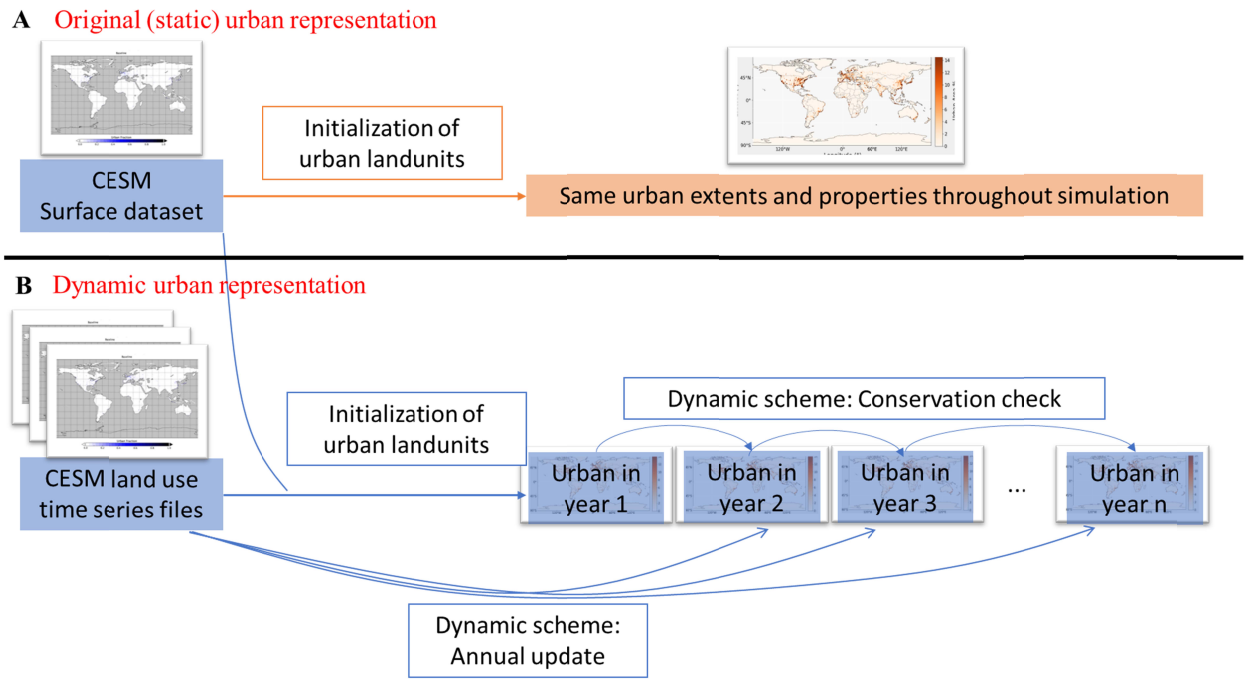

Figure 3. Comparison of existing urban representation and the proposed novel urban scheme. ***A:*** *existing urban representation where, once initialized, urban extents and properties remain constant throughout the simulation.* ***B:*** *dynamic urban scheme, where the model initializes urban in select regions, and urban extents are updated annually according to the input data while conserving energy and mass balance.*

To add the transient land use capability for urban land units, our new dynamic urban scheme reads a land use time series dataset that prescribes the percent cover of the three urban land units each year and updates the urban land units throughout the simulation accordingly. The changes in urban area extent in time are integrated with changes in other land units in the model (Figure 1C). The following sections describe the implementation of the dynamic urban scheme in more detail.

3.1 Dynamic urban land data

In the default configuration of CLMU, a global dataset (J2010) provides present-day (circa-2000) information on urban spatial extent (i.e., percent cover within a grid cell), urban morphological (e.g., building height, street width, building height-to-street width ratio. roof areal fraction, and pervious canyon floor fraction), thermal (e.g., material heat capacity and thermal conductivity), and radiative (e.g., albedo and emissivity) properties. The spatial extent of urban areas is derived from a population density dataset at 1-km resolution, and the relative weights of different urban density types are based on population and satellite imagery. The dataset defines 33 unique regions globally, grouped according to similar urban surface properties. The urban property data are compiled by synthesizing a variety of datasets, including satellite products, a global database of tall buildings, local building codes data and other municipal documentation, and validated against Google Earth imagery (Jackson et al., 2010). These properties have been updated somewhat as described in Oleson and Feddema (2020).

The new dynamic urban scheme requires future urban land projection datasets under different

scenarios. Recent efforts in global-scale spatial projections of urban land change provide the necessary source data. These time series of global urban land projections use remote sensing and population density data and leverage existing regional/zonal modeling methods (G. Chen et al., 2020; Gao & O'Neill, 2020; He et al., 2021; Z. Liu et al., 2019) to better captures the regional heterogeneity in urban development trajectory. Here we generated two CESM-compatible transient urban land use time series data based on two urban land cover projection datasets – Gao and O'Neill (2020) (hereinafter **GO2020**) and He et al. (2021) (Supplementary Information; hereinafter **BNU**), aiming to demonstrate the validity of our new dynamic urban scheme. The BNU and GO2020 datasets provide the global urban land cover between 2020 - 2070 and 2010 - 2100, respectively, in decadal intervals under five CMIP6 ScenarioMIP (O'Neill et al., 2016) Shared Socioeconomic Pathways (SSPs) at a 1-km resolution. The historical urban land cover in the year 2000 is also available in the GO2020 dataset.

CESM provides the infrastructure for users to process input data, which includes the THESIS (Toolbox for Human-Earth System Integration and Scaling) tool to create the raw urban extent and urban properties datasets and the CTSM *mksurfdata_esmf* tool to create surface datasets and land use time series datasets at the desired spatial resolution for model simulation (Oleson and Feddema, 2020). Here we use the THESIS tool to combine the 1-km urban land cover data with urban properties and then aggregate the urban extent to 0.05° resolution (Figure 4). The original THESIS tool described in Oleson and Feddema (2020) only accepts binary urban land cover input but has been modified in this work to accept generic data format. It assumes that the input urban land cover data is urban fraction with respect to the grid cell area (e.g., as provided by the GO2020 dataset). At this point, all urban areas are assumed to be MD. The land use time series

304 file compatible with CLMU's configuration requires three urban density types (TBD, HD, and
305 MD). Thus, the 0.05° urban land cover files need to be further divided into these three density
306 classes. The partitioning we use here references the J2010 urban dataset and is based on the
307 following rules and assumptions.

308

309 At the beginning of the time series, the urban area in each grid cell is partitioned according to the
310 ratio of the density types in that grid cell in the J2010 dataset. If an urban land unit later grows or
311 shrinks, the area of each urban density type increases or decreases proportionally. If a new urban
312 land unit appears at any point in time (either at the start of the time series or later) in a grid cell
313 where urban does not previously exist in the J2010 dataset, the percentages of the three density
314 types are assigned to the average value in the "region" that the grid cell belongs to. Here the
315 "region" refers to the 33 physically and socially unique zones defined in J2010. These rules
316 essentially assume that the morphology of an emerging urban area will resemble other cities in
317 its vicinity.

318

319 Then, the decadal 0.05° urban data were linearly interpolated to generate annual urban data files
320 from 2020 to 2070 for the BNU dataset and from 2015 to 2100 for the GO2020 dataset. The
321 historical annual urban data from 2000 to 2015 is also created for the GO2020 dataset. In this
322 process, the average urban fraction of the five SSP scenarios was calculated in 2010 and 2015,
323 respectively, which is used as the historical urban land cover for those two years. Then the
324 annual urban fraction from 2000 to 2015 were interpolated based on historical urban fraction in
325 2000, 2010, and 2015.

Finally, the 0.05° urban data from 2000 to 2100 and data files of other land cover types are ingested by the *mksurfdata_esmf* tool to create a surface dataset in the year 2000 and a land use time series dataset for the period of 2000 – 2100 at the desired spatial resolution for model simulation (Oleson and Feddema, 2020). Since the BNU datasets only provide urban data from 2020 to 2070, the urban land cover from 2000 to 2019 takes the values of 2020 and the urban land cover after 2070 is fixed at the 2070 level. Here the *mksurfdata_esmf* tool has been modified to include annual urban fractions in the land use time series files. To reconcile the area change of urban with other land use types, we make the following informed assumption. In the case of a decrease in the urban area, the urban area would transform into natural vegetation and bare soil (i.e., vegetated land unit). As for urban expansion, cities will first replace natural vegetation and bare soil, and then cropland. Cropland is assigned higher priority based on our view that food security will continue to be a priority given the growing population (J. Chen et al., 2017; Gregory et al., 2005; Vermeulen et al., 2012). Note that in the original BNU dataset, urban area can shrink at certain future time points as the projected urban population decreases. Here we make a "non-decreasing" urban area assumption that the urban fraction will be kept at the previous decadal level if the BNU data predicts it to shrink. This is a reasonable assumption because in reality, the physical urban landscape would not necessarily be converted back to vegetated landscapes even if the urban population decreases. The GO2020 dataset does not have shrinking urban areas.

To summarize, the process to generate a land use timeseries dataset with transient urban land is as follows: First, we use the THESIS tool to combine the decadal 1-km resolution urbanization

projections with urban properties and upscale it into an urban fraction dataset at 0.05° resolution. Then we classify the urban area further into three density types and interpolate the decadal urban fraction datasets to annual data. Finally, we use the annual urban data as the input to the *mksurfdata_esmf* tool to generate the surface dataset in 2000 and the land use time series dataset for the period of 2000 – 2100. The surface datasets and land use time series datasets based on the GO2020 data under five SSPs scenarios are made available for users at 0.9° × 1.25° resolution, however, datasets at other resolutions can be created using the *mksurfdata_esmf* tool. This workflow (Figure 4) has been incorporated in the modified THESIS and *mksurfdata_esmf* tools which are published open-source (see Data and Code Availability statement) along with this paper. With these tools users can also convert an urbanization projection of their preference into datasets compatible with CESM and thus dynamically simulate the climate effects of urbanization according to that projection.

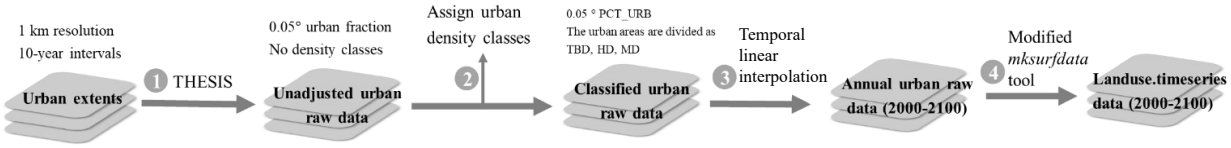

Figure 4. Illustration of the process and tools for urban transient land use dataset processing.

The resulting urban cover in the surface dataset and the land use time series are expressed in the form of each urban density type's fractional areal weights relative to the land fraction of the grid cell. Figure 5 demonstrates the urban land change from the land use timeseries dataset at 1 degree resolution, based on BNU projection. The total urban area increases by 82% from 2015 to

2070 (from 8.9×10^5 km^2 to 1.6×10^6 km^2), with TBD, HD and MD increasing by 8.7%, 48% and 91% respectively. There are 3,657 and 4,291 grid cells with urban areas in 2015 and 2070, respectively. 4,245 grid cells see expansion in urban areas from 2015 to 2070.

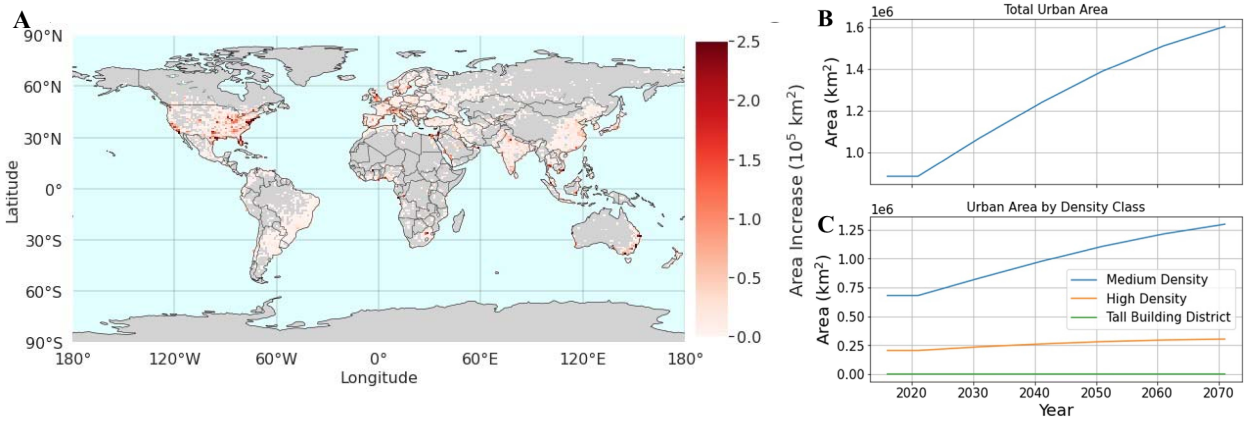

Figure 5. Global urban expansion, according to BNU projection, SSP5 scenario. ***A:*** *Urban area change from 2015 to 2070. Right: Projected global total urban area (**B**) and areas of each urban density class (**C**), in 10^6 km^2. Projection starts from 2020.*

3.2 Dynamic urban module

In the dynamic urban scheme, the model updates the extent of urban areas each year from the new land use time series file described above. We modified the model input/output (I/O) interface to supply the urban extent information from urbanization land use time series, rather than from a static surface dataset in the current version of CLMU. The dynamic urban module updates the urban extents at the beginning of each model year (**Figure 3B**). As a special consideration, if the timespan of a simulation is longer (at beginning or end) than that of the urbanization time series, the first time slice in the data is used to define the urban extent for all model years prior to that year, and similarly the last time slice in the data applies to all model

years after that year.

Urbanization can be realized through either the expansion of existing urban areas or the emergence of new urban areas from formerly rural or unmanaged land. In the former scenario, urban growth is represented as growth in urban extent in the same grid cell, or more specifically, as an increase in the urban land unit weight within the grid cell. The newly developed urban area maintains the same state variables as the existing urban area and therefore forms a smooth transition. The latter situation, however, involves establishing a new urban land unit in a grid cell, and consequently poses an initialization problem. Like other land use types, the urban representation in CTSM involves biophysical processes that require interactions with the atmospheric forcing. After the simulation has started, it is not feasible to initiate new urban land units with the proper initial state, and an urban land unit with a "cold start" state would not be in equilibrium with past atmospheric forcing. One possible solution is to initialize all three urban land units virtually in grid cells where there is no urban landscape at the start of the simulation, calculate all the urban processes along the way, and set urban to zero area weight if no new urban land emerges in later years so that they don't influence the surface fluxes sent to the atmosphere. This solves the initialization problem but is computationally inefficient. To improve the computing efficiency, we only initialize urban land units where urban areas already exist or will emerge later in the simulation. This is done by pre-examining the transient urban land use time series to determine the maximum fraction of urban area at each grid cell across the entire timespan. The model then reads this maximum urban percentage information and initializes and runs urban columns only where necessary. A grid cell with zero maximum indicates that an urban land unit will never emerge in this grid cell throughout the simulation period and therefore

410 the urban initialization will not be invoked. Our testing results indicate this procedure leads to
411 more than 10% improvement in model efficiency compared to the all-active zero-weight urban
412 method.

413

414 Similar to other dynamic land units, this dynamic urban feature can be switched off in the case
415 configuration phase when a simulation with static urban extent is desired.

416

417 **3.3 Energy and water conservation in land conversion**

418 Urbanization – land use conversion from natural vegetated or crop to urban land unit – can cause
419 failures of mass and energy conservation in the model. CTSM has an existing mechanism to
420 handle the energy and mass (water, carbon, and nitrogen) conservation for certain types of land
421 use transitions (conversion between vegetation, crop, and glacier land units). We leverage the
422 existing mechanism and, with several necessary modifications, extend it to handle urban land
423 changes.

424

425 For energy conservation, the model assumes that when land unit areas change, the state variables
426 remain constant on a per-area basis, which may lead to changes in total grid cell energy content.
427 For example, if an urban land unit has a higher value in heat content (expressed in $J \cdot m^{-2}$) than
428 another landunit, and when the former expands and replaces part of the latter, they each retain
429 their heat content values, leading to a net increase energy in the grid cell. This artificial change
430 will violate the surface energy balance in the model if not accounted for. To account for such
431 discrepancy caused by land use conversion, a fictional "balancing flux" has been introduced to

balance any change. The flux is distributed evenly throughout the whole year following the land use change to avoid any large or abrupt changes.

For water, we treat liquid water and ice separately and use a similar approach as energy. Specifically, the model keeps the pre-conversion per-area water contents for different land use types at the same level, and we account for the water content differences due to the conversion with "water balancing fluxes". For example, if urbanization leads to water loss, we create an outgoing flux (represented as runoff) to fix the discrepancy. Note that the energy transfer associated with the water or ice balancing fluxes are also considered in the energy balance.

Testing results demonstrate that both water and energy are properly conserved with this treatment. After the balancing fluxes are accounted for, the remaining imbalances are below the specific energy and water balance thresholds used in the model and are thus considered negligible. An example of the residual in water and energy balance after correction for year 2020 is shown in Figure 6 and Table 1 (for the simulation described in section 4). After urban extents change at the beginning of the year, there is change in global average liquid water content of 0.034 mm at the beginning of the year due to urban land cover change. An adjustment of $1.1 \times 10^{-9}\ mm \cdot s^{-1}$ (global average; the actual adjustment is applied individually to each grid cell) to the global runoff throughout the following year balances the liquid water content to $3.0 \times 10^{-7}\ mm$ (Figure 6B). Similarly, there is a change in the global average heat content at the beginning of the year of $-46\ kJ \cdot m^{-2}$, consisting of a change in heat content of $21\ kJ \cdot m^{-2}$ and a change in heat content contained in the runoff ($-67\ kJ \cdot m^{-2}$). An adjustment to the global sensible heat flux of $3.3 \times 10^{-4}\ W \cdot m^{-2}$ throughout the following year correct corrects this to

$-1.8\ kJ \cdot m^{-2}$ (Figure 6A), a value that is much smaller compared to the average global heat content of $3.1 \times 10^5\ kJ \cdot m^{-2}$. We have checked every grid cell in our simulation and confirmed that the errors after correction meet our balance criteria.

Table 1. Global average of imbalance before and after "balancing flux" correction at the beginning of year 2020.

Quantity	Global average discrepancy		Balancing flux
	Before correction	After correction	
Liquid content	3.4×10^{-2} mm	3.0×10^{-7} mm	1.1×10^{-9} mm·s^{-1}
Ice content	6.6×10^{-5} mm	-1.6×10^{-8} mm	2.1×10^{-12} mm·s^{-1}
Heat content	-46 kJ/m^2	-1.8 kJ/m^2	3.3×10^{-4} W·m^{-2}

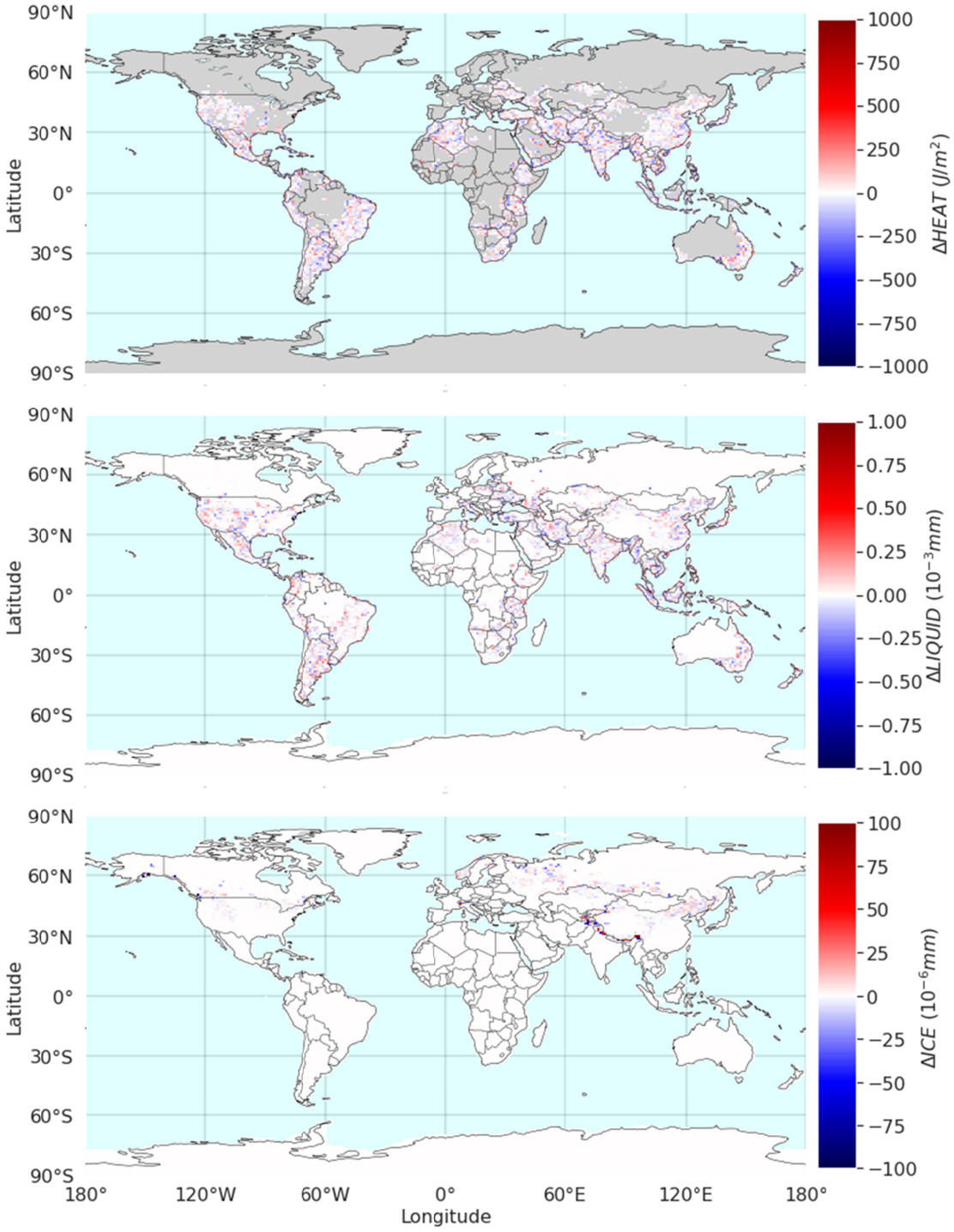

462

463 **Figure 6. Water and energy discrepancy throughout land use change after the adjustment**

464 **by "balancing fluxes".** ***A, B*** *and* ***C*** *are grid-cell changes in heat (including latent heat in runoff),*

465 *water and ice, respectively, when the land use change happens at the beginning of 2020.*

We note that the urban land unit does not model carbon and nitrogen in the current version of the model and therefore we only account for changes in energy and water. Our new scheme does track the carbon and nitrogen change associated with urban land change for mass conservation purpose in the model. The carbon and nitrogen will be stored when urban land unit replacing vegetated or crop land and will be released when vegetated or crop replaces urban. The stored carbon and nitrogen are treated as inert pools and can be properly conserved in the model with this method.

4. Dynamic-urban simulation results and discussion

Using a standard test suite available as part of CTSM, the new dynamic-urban scheme has passed the tests that check for proper operation under a large range of possible CESM model setups and conditions, including evaluation of performance (speed), memory, and I/O. To further illustrate the application and function of the new scheme, we conducted a pair of land-only simulations. These simulations are for the purpose of demonstrating the validity of the dynamic-urban scheme, rather than projecting future urban climates under climate change and urbanization, because land-atmosphere interactions and feedbacks are not represented in these uncoupled runs.

The two simulations were run from 2015 to 2070 at a spatial resolution of 0.9^{o} latitude x 1.25^{o} longitude, one with constant urban land cover (StaticUrban) and the other with the dynamic urban scheme (DynamicUrban). The atmospheric forcing data is taken from atmospheric output from a fully coupled simulation under a very high-emission Shared Socioeconomic Pathway-Representative Concentration Pathway scenario, SSP5-8.5. Except active river model, other

488 model components of CESM are in their data modes (stub ice, ocean, wave, and glacier (land
489 ice)). For illustrative purpose, only the DynamicUrban simulation with the BNU projection data
490 is shown here.

491

492 The simulation results confirm that our new dynamic urban scheme functions properly in the
493 CESM modeling framework and demonstrate the direct local climate effects of urban expansion
494 (**Figure 7**). These effects are shown as grid-cell level differences between DynamicUrban and
495 StaticUrban runs, averaged during 2061-2070. Because there are no feedbacks from land to the
496 atmosphere in the land-only simulations, the grid-cell mean differences between the two runs are
497 essentially caused by the changes in area weights of urban land units in the model (i.e.,
498 urbanization). The urban subgrid climate outputs (state and flux variables) do not differ when the
499 urban extent changes under the identical climate forcings between the two runs. Urban
500 expansion is shown to cause an almost consistently higher 2-m temperature (T_a) in the grid cells
501 with expanding urban landscape, with an average difference of 0.0124 ± 0.008 K (mean ± 95%
502 confidence intervals (CI)) compared to the static urban case (**Figure 7A**). This is essentially
503 because the temperature of emerging urban area is higher than that of the landscape being
504 replaced (urban heat island effect, Zhao et al., 2014). Our results also show a near-universal
505 decrease in 2-m relative humidity (RH) in grid cells with expanded urban area, with an average
506 absolute difference of -0.0762 ± 0.0046% (**Figure 7B**). This is largely due to the large fraction of
507 impervious surfaces in urban areas replacing the original permeable landscapes (such as bare soil,
508 vegetated, or crop land) which reduces the surface evapotranspiration. Empirical observational
509 evidence exists for such an urbanization-induced decrease in local RH in recent decades (W. Liu
510 et al., 2009; Luo & Lau, 2019; Meili et al., 2022). The loss of pervious surfaces during urban

expansion channels more available energy to surface convection rather than evapotranspiration, as evidenced by increased sensible heat flux (SH) and decreased latent heat flux (LE) over most urbanized areas (**Figure 7C** and **7D**). The average SH for grids with urban expansion is 0.151 ± 0.013 Wm^{-2} higher in DynamicUrban than StaticUrban. For latent heat, the difference is -0.116 ± 0.011 Wm^{-2}.

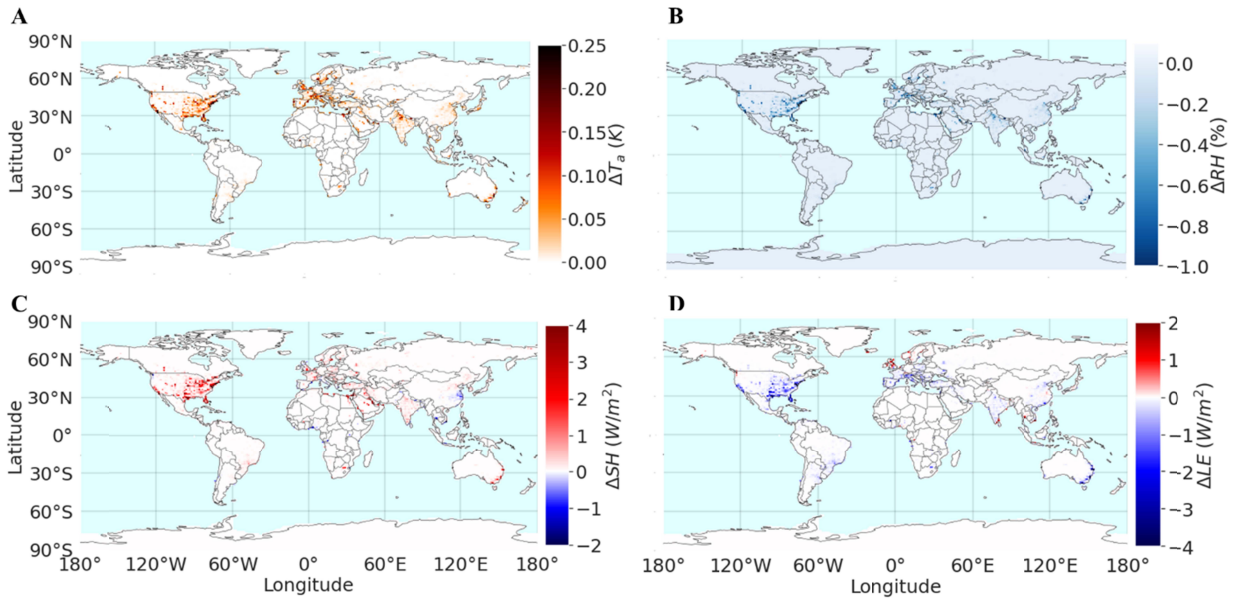

Figure 7. The direct local climate effect of urbanization as represented by the BNU dataset. *Plots demonstrate the difference in 2-meter air temperature (ΔT_a), **(A)**, relative humidity (ΔRH), **(B)**, sensible heat (ΔSH)and latent heat (ΔLE), **(C, D)** between dynamic urban and static urban simulations. Differences are grid-cell average values for 2061 to 2070.*

These direct climate effects are most pronounced in regions where there are both already high urban fractions (since urban area has more weights in the grid cell) and significant projected urban expansion (e.g., United States, West Europe, coastal Australia). Because the simulations

526 are uncoupled, the magnitude of the direct climate effect is roughly proportionate to the change
527 in urban extent. Examples can be illustrated by the local (urban subgrid) and regional (grid cell
528 average) warming in Southern California, US, and Sydney, Australia (Figure 8). Both regions are
529 projected to experience extensive urbanization (denoted by the increasing dot sizes) and urban
530 warming (color of the dots) in the coming decades. The direct effects shown in grid-cell average
531 temperatures increase with the increase of urban extent. The local urban (subgrid) warming is
532 purely from the climate change signal from the forcings in our offline simulations. If a fully
533 coupled simulation (e.g., active atmosphere) is conducted, we expect "indirect" climate effects
534 from urbanization which, through land-atmosphere interaction and feedbacks, further alter local
535 urban and regional climate.

536

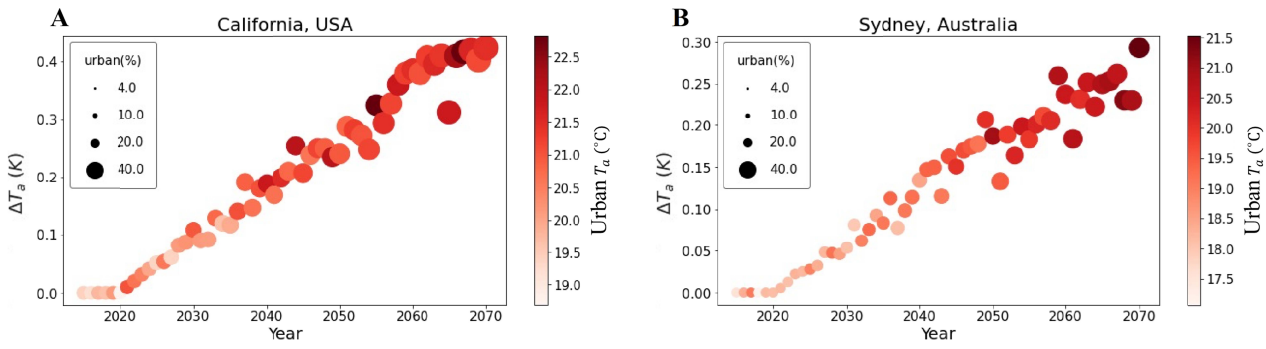

537
538

539 **Figure 8. Local urban and regional warming effects of urbanization under climate change.**
540 ***A*** *(South California, USA, urban region within 150-152 °E, 32-35 °S) and* ***B*** *(Sydney, Australia,*
541 *urban region within 117-119 °W, 32.5-35.5 °N) are two cases showing the local and regional*
542 *warming effects. Left Y-axis indicates the grid-cell average warming caused by urbanization.*
543 *Color denotes local urban temperature (right Y-axis), and symbol size denotes urban expansion*
544 *(percentage of area change compared to 2015). Urbanization projection (BNU data) starts from*

2020, and urban extent is kept at present-day level between 2015 and 2020.

5. Conclusion

We develop and implement a new dynamic urban scheme in CESM, making it the first Earth system model that has a transient representation of future urbanization. The new dynamic urban feature not only makes the urban land use change in the model consistent with the greenhouse gas emission trajectories, but also extends the modeling capability to dynamically simulate the climate effects induced by both urbanization and global climate change. Urban areas are often converted from natural vegetation or cropland. The consequential changes in surface properties including addition of impervious surfaces and loss of natural vegetation or cropland, would pose significant influence on local and regional climates. These landscape modifications also alter the land-atmosphere interactions and deliver indirect climate impacts across scales. The implementation of the dynamic urban feature is the first step moving forward. The new dynamic-urban CESM out of this study provides critical opportunities to advance understanding of how global-scale greenhouse gas warming coupled with urbanization affects local- and regional-scale climates, a critical question shaping the Earth's sustainable future. The new dynamic urban scheme has been released in the latest development version of CTSM (https://github.com/ESCOMP/CTSM).

Fully coupled simulations with our new dynamic CESM could offer more insights towards mechanistical understanding of the hydroclimatological impacts of urbanization and climate change. As the next steps in future work, further improvements will be made to the input data of

this dynamic CESM/CTSM. Specifically, the dynamic urban land time series will be extended back to cover the full historical period (since 1850). Besides, proportions of the three urban density types (TBD, HD and MD) in future projected urban land could be refined using additional data (e.g., future population distribution data), instead of simply being inherited from J2010.

Code and Data Availability

The code of the new dynamic urban scheme is publicly available in the latest development version of the Community Terrestrial System Model (CTSM) via its git repository (https://github.com/ESCOMP/CTSM). The modified THESIS urban properties tool and *mksurfdata_esmf* tool are available at https://figshare.com/s/4a890655b34498c1d082 (DOI: 10.6084/m9.figshare.22680331). The two CESM-compatible transient urban land use time series datasets (i.e., GO2020- and BNU-based) are available from the CESM input data repository on NCAR's Cheyenne cluster as an optional surface data input for CTSM/CLMU.

Acknowledgments

L.Z. acknowledges the support by the U.S. National Science Foundation (CAREER Award Grant No. 2145362) and the Institute for Sustainability, Energy, and Environment at the University of Illinois Urbana-Champaign. We acknowledge the high-performance computing support from Cheyenne (https://doi.org/10.5065/D6RX99HX) provided by NCAR's Computational and Information Systems Laboratory, sponsored by the U.S. National Science Foundation. The authors declare no conflict of interest.

Appendix

Supplemental Material

In the derivation of the building energy model (BEM) in Oleson and Feddema (2019) an assumption was made that the building width is equal to the street width. Here however, this assumption has been relaxed and building width is now derived from the data in the Jackson et al. (2010) morphology dataset. Specifically, the BEM equations which use H/W_S (building height to street width ratio) now use H/W_B (building height to building width ratio). Building width is $W_B = W_S W_{roof} / \left(1 - W_{roof}\right)$ where W_{roof} is roof fraction.

The BEM equations are modified as follows. Following the derivation in Oleson and Feddema (2020) (Eqs. 1-6), an energy balance is constructed for each interior surface and indoor air as

$$F_{rd,roof} + F_{cv,roof} + F_{cd,roof} = 0 \quad (1)$$

$$F_{rd,sunw} + F_{cv,sunw} + F_{cd,sunw} = 0 \quad (2)$$

$$F_{rd,shdw} + F_{cv,shdw} + F_{cd,shdw} = 0 \quad (3)$$

$$F_{rd,floor} + F_{cv,floor} + F_{cd,floor} = 0 \quad (4)$$

$$V_B \rho C_p \frac{\partial T_{iB}}{\partial t} - \sum_{sfc} A_{sfc} h_{cv,sfc} \left(T_{ig,sfc} - T_{iB}\right) - \dot{V}_{vent} \rho C_p \left(T_{ac} - T_{iB}\right) = 0 \quad (5)$$

where F_{rd} is the net longwave radiation (W m^{-2}), F_{cv} is the convection flux (sensible heat flux), and F_{cd} is the heat conduction flux (W m^{-2}) for each surface. In Eq. (5), V_B is the volume of building air (m^3), ρ is the density of dry air at standard pressure P_{std} and indoor air

609 temperature T_{iB} ($\rho = P_{std}/R_{da}T_{iB}$ where $P_{std} = 101325$ Pa and $R_{da} = 287.04$ J K^{-1} kg^{-1} is the dry

610 air gas constant), $C_p = 1.00464 \times 10^3$ is the specific heat of dry air (J kg^{-1} K^{-1}), A_{sfc} is the area

611 (m^2), $h_{cv,sfc}$ is the convective heat transfer coefficient (W m^{-2} K^{-1}), and $T_{ig,sfc}$ is the interior

612 surface temperature of each surface (subscript *sfc* is roof, sunw, shdw, or floor). The last term in

613 Eq. (5) represents exchange of indoor air and outdoor air in the urban canyon where $\dot{V}_{vent}$ is the

614 ventilation air flow rate (m^3 s^{-1}) and T_{ac} is the urban canopy layer air temperature (K).

615

616 Since $V_B = W_B LH$ (m^3), $A_{roof} = A_{floor} = W_B L$ (m^2), and $A_{sunw} = A_{shdw} = HL$ (m^2), where W_B is

617 building width (m), H is building height (m), and L is building length or depth (m), Eq. (5)

618 can be rewritten as

619
$$H\rho C_p \frac{\partial T_{iB}}{\partial t} - h_{cv,roof}\left(T_{ig,roof} - T_{iB}\right) - h_{cv,floor}\left(T_{ig,floor} - T_{iB}\right) - \frac{H}{W_B} h_{cv,sunw}\left(T_{ig,sunw} - T_{iB}\right) - \frac{H}{W_B} h_{cv,shdw}\left(T_{ig,shdw} - T_{iB}\right) - \left(\frac{ACH}{3600}\right) H\rho C_p \left(T_{ac} - T_{iB}\right) = 0 \quad (6)$$

620 where ventilation is represented by ACH, the number of air exchanges between indoor and

621 outdoor volume of air per hour.

622

623 The view factors between surfaces used in determining the net longwave radiation for each

624 interior surface as described in Text S1 in Oleson and Feddema (2019) are also modified as

625
$$\Psi_{floor-roof} = \sqrt{1 + \left(\frac{H}{W_B}\right)^2} - \frac{H}{W_B} \quad (7)$$

$$\Psi_{wall-floor} = \frac{1}{2}\left(1 - \Psi_{roof-floor}\right) \quad (8)$$

$$\Psi_{floor-wall} = \frac{\Psi_{wall-floor}}{H/W_B} \quad (9)$$

$$\Psi_{roof-wall} = \Psi_{floor-wall} \quad (10)$$

$$\Psi_{wall-roof} = \Psi_{wall-floor} \quad (11)$$

$$\Psi_{wall-wall} = 1 - \Psi_{roof-wall} - \Psi_{floor-wall}\,. \quad (12)$$

Note that for $W_{roof} = 0.5$, $W_B = W_S$, the assumption in the original version of the model.

Second, the effects of ventilation (exchange of building air with canopy air) as described in Oleson and Feddema (2020) are accounted for in the energy budget inside the building as shown in Eq. (5) where $\dot{V}_{vent}$ is the ventilation air flow rate ($m^3\ s^{-1}$). However, the opposite and equal flux to the urban canyon was not accounted for. The following remedies that omission and the sensible heat flux into the urban canyon due to ventilation (H_{vent}) is added to the canyon floor similar to the sensible heat due to wasteheat and the heat removed by air conditioning. Following equation 4.26 in (Oleson et al., 2010), the sensible flux into each urban surface h is now

$$h = \vec{S}_g - \vec{L}_g - H_g - \lambda E_g + H_{wasteheat,g} + H_{aircond,g} + H_{vent,g} \quad (13)$$

where $\vec{S}_g$ is the absorbed solar radiation, $\vec{L}_g$ is the net longwave radiation, and H_g and λE_g are the sensible and latent heat fluxes, all in W m^{-2}. The terms $H_{wasteheat,g}$, $H_{aircond,g}$, and $H_{vent,g}$ are

644 the wasteheat from space heating/air conditioning, the heat removed by air conditioning, and the
645 ventilation heat flux, respectively, applied only to the pervious (prvrd*)* and impervious canyon
646 floor (imprvrd*)*

$$
\begin{aligned}
&H_{wasteheat,prvrd} = H_{wasteheat,imprvrd} = \frac{H_{wasteheat}}{1-W_{roof}} \\
&H_{wasteheat,sunwall} = H_{wasteheat,shdwall} = H_{wasteheat,roof} = 0 \\
&H_{aircond,prvrd} = H_{aircond,imprvrd} = \frac{H_{aircond}}{1-W_{roof}} \\
&H_{aircond,sunwall} = H_{aircond,shdwall} = H_{aircond,roof} = 0 \\
&H_{vent,prvrd} = H_{vent,imprvrd} = \frac{H_{vent}}{1-W_{roof}} \\
&H_{vent,sunwall} = H_{vent,shdwall} = H_{vent,roof} = 0
\end{aligned}
\tag{14}
$$

647

648 where $H_{wasteheat}$ and $H_{aircond}$ are the total waste heat and heat removed by air conditioning.

649 H_{vent} is the total ventilation heat flux (see Eq. (6))

$$
H_{vent} = W_{roof}\left(\frac{ACH}{3600}\right)H\rho C_p\left(T_{iB} - T_{ac}\right). \tag{15}
$$

650

651

652 Oleson and Feddema (2020) reported on results using the BEM from a global land-only (with
653 CLM uncoupled from an active atmospheric model) simulation (CLM5_UPV2_BEMV2). Here,
654 a new historical simulation (CLM5_UPV2_BEMV3) that includes the two modifications
655 described above was conducted for 1850-2005 using CLM5
656 (https://github.com/ESCOMP/CTSM/releases/tag/clm5.0.dev010). The results for 1986-2005
657 are compared to the original simulation to assess the combined effects of the modifications on
658 urban canopy air temperature and anthropogenic heat flux (AHF).

659

660 Following the analysis in Oleson and Feddema (2020), the spatial pattern of differences in mean
661 (Tmean), daily maximum (Tmax) and minimum (Tmin) urban canopy air temperature and AHF
662 components for CLMU_UPV2_BEMV3 compared to CLM5_UPV2_BEMV2 are shown in
663 Figure S1, with a summary of global average AHF components in Table S1. These results
664 reflect the weighted (by area) average of the three urban density types [tall building district
665 (TBD), high density (HD), and medium density (MD)]. In general, the modification to use the
666 derived W_B decreases Tmean over most regions while the H_{vent} modification increases Tmean
667 (not shown). The increase in Tmean is larger than the decrease such that the combined change in
668 Tmean is about 0.02 °C averaged globally (Figure S1). The largest increases are associated with
669 the TBD density type which has the largest building air volume (differences are 0.0°C to 0.35°C
670 depending on region; not shown). Changes for Tmin are larger than for Tmax mainly because
671 the building interior is warmer than canopy air at night, particularly in winter, and there is a
672 positive sensible heat flux into the urban canyon due to the H_{vent} modification.
673
674 Figure S1 and Table S1 indicates there is an increase in AHF released into the climate system
675 from the modifications. Global AHF for 1986-2005 increases slightly from 3.47 TW to 3.56 TW
676 (~3%). Most of this is due to an increase in space heating due to the use of the derived W_B. In
677 regions that require space heating in winter, heating increases for $W_{roof} < 0.5$ (primarily the
678 medium density type which has the largest area) and decreases for $W_{roof} > 0.5$ (primarily the
679 TBD density type which has the smallest area).
680

Figure S2 indicates that the simulated AHF still compares well with an estimate from Flanner (2009) over the U.S. with a slight degradation in the pattern correlation. On the other hand, the positive bias in the model over Europe (Figure S3) increases from about 0.08 TW to 0.20 TW indicating that the building properties may need to be revisited in this region (e.g., an increase in roof and/or wall insulation would reduce space heating demand).

In summary, the changes in urban canopy air temperature and anthropogenic heat flux due to these modifications are generally relatively small, although they can be significant depending on certain combinations of density type, urban morphology, season, and climate.

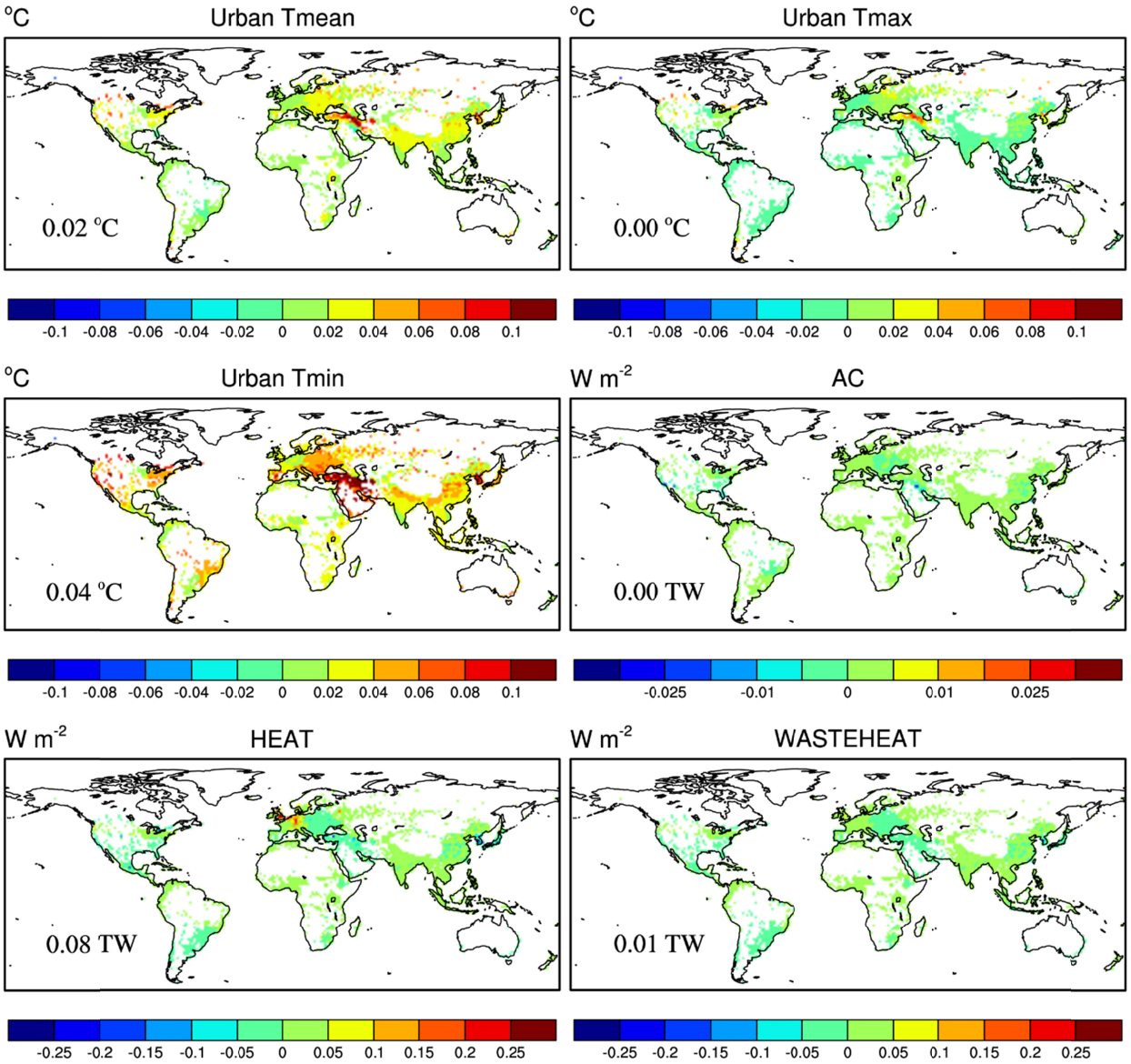

Figure S1. Differences in annual mean (Tmean), daily maximum (Tmax) and minimum (Tmin) urban canopy air temperature, air conditioning (AC), space heating (HEAT), and wasteheat between the CLMU_UPV2_BEMV3 and CLMU_UPV2_BEMV2 simulations for 1986-2005. Numbers in the lower left corner of the plots for Tmean, Tmax, and Tmin represent the global mean difference (°C) and the numbers for AC, HEAT, and WASTEHEAT represent the global total difference (TW).

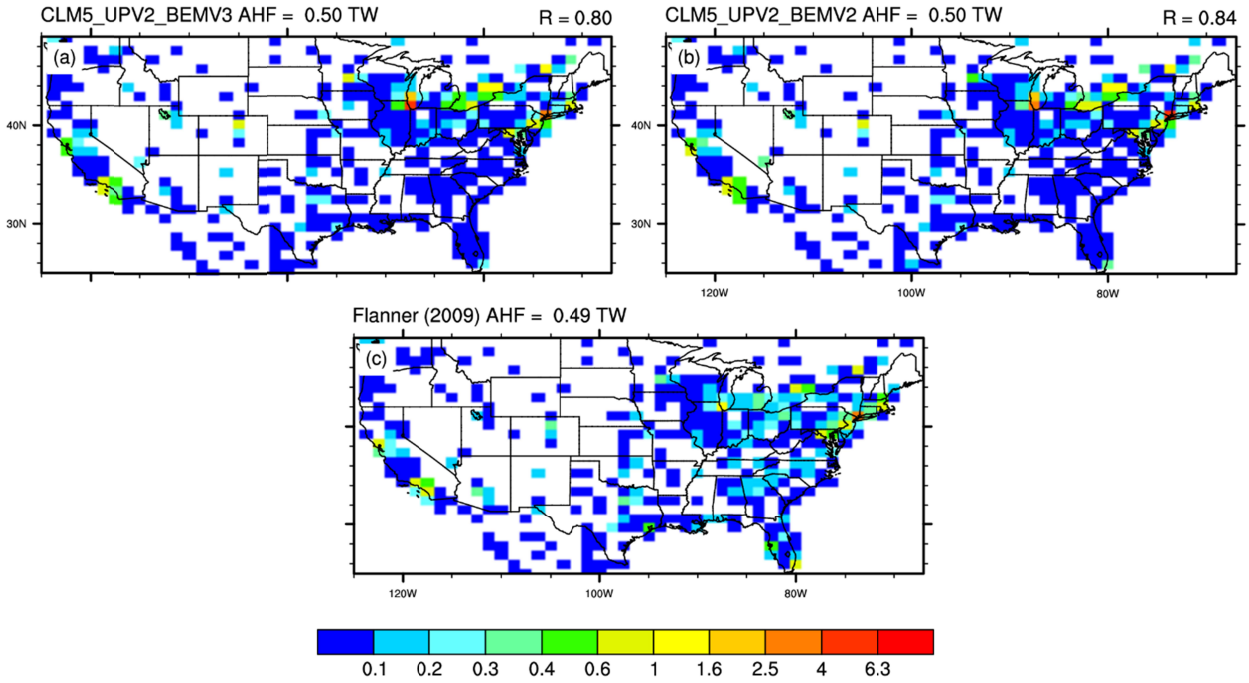

Figure S2. Comparison of anthropogenic heat flux (AHF) due to space heating and air conditioning over the U.S. from the (a) CLM5_UPV2_BEM3, and (b) CLM5_UPV2_BEM2 simulations, and (c) Flanner (2009) dataset (W m^{-2}). The Flanner (2009) total AHF from all sources has been multiplied by 16% to adjust it for energy due only to space heating and air conditioning (Oleson and Feddema, 2020). The model and Flanner (2009) data have been masked for each other's urban areas. R is the pattern correlation between the model simulations and Flanner (2009).

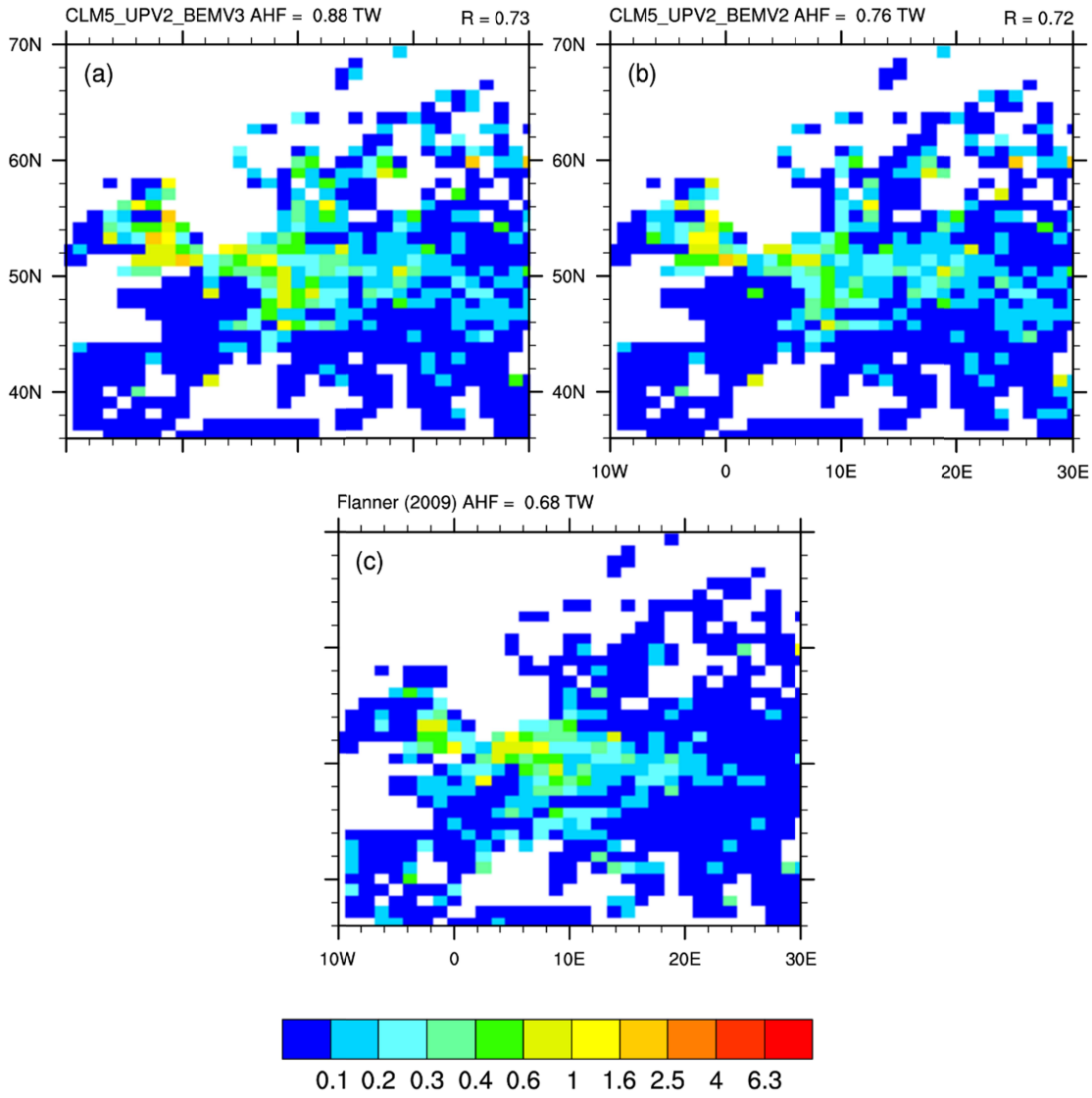

Figure S3. As in Figure S2 but for Europe. The Flanner (2009) total AHF from all sources has been multiplied by 25% to adjust it for energy due only to space heating and air conditioning (Oleson and Feddema, 2020).

Table S1. Global urban air conditioning (AC), space heating (HEAT), wasteheat (WSTH), and total anthropogenic heat flux (AHF) (all in terrawatts) for 1986-2005 for the simulations described in the text. The AHF is calculated as HEAT plus WSTH.

	AC	HEAT	WSTH	AHF
CLM5_UPV1_BEMV2	0.03	2.88	0.59	3.47
CLM5_UPV2_BEMV3	0.03	2.96	0.60	3.56

718 **Reference**

719 Baklanov, A., Grimmond, C. S. B., Carlson, D., Terblanche, D., Tang, X., Bouchet, V., et al.
720 (2018). From urban meteorology, climate and environment research to integrated city
721 services. *Urban Climate*, *23*, 330–341. https://doi.org/10.1016/j.uclim.2017.05.004
722 Bren d'Amour, C., Reitsma, F., Baiocchi, G., Barthel, S., Güneralp, B., Erb, K.-H., et al. (2017).
723 Future urban land expansion and implications for global croplands. *Proceedings of the*
724 *National Academy of Sciences*, *114*(34), 8939–8944.
725 https://doi.org/10.1073/pnas.1606036114
726 Cao, C., Lee, X., Liu, S., Schultz, N., Xiao, W., Zhang, M., & Zhao, L. (2016). Urban heat
727 islands in China enhanced by haze pollution. *Nature Communications*, *7*(1), 12509.
728 https://doi.org/10.1038/ncomms12509
729 Chakraborty, T., Hsu, A., Manya, D., & Sheriff, G. (2019). Disproportionately higher exposure
730 to urban heat in lower-income neighborhoods: a multi-city perspective. *Environmental*
731 *Research Letters*, *14*(10), 105003. https://doi.org/10.1088/1748-9326/ab3b99
732 Chen, G., Li, X., Liu, X., Chen, Y., Liang, X., Leng, J., et al. (2020). Global projections of future
733 urban land expansion under shared socioeconomic pathways. *Nature Communications*,
734 *11*(1), 537. https://doi.org/10.1038/s41467-020-14386-x
735 Chen, J., McCarl, B. A., & Thayer, A. (2017). Climate Change and Food Security: Threats and
736 Adaptation. In *World Agricultural Resources and Food Security* (Vol. 17, pp. 69–84).
737 Emerald Publishing Limited. https://doi.org/10.1108/S1574-871520170000017006
738 Creutzig, F., Baiocchi, G., Bierkandt, R., Pichler, P.-P., & Seto, K. C. (2015). Global typology of
739 urban energy use and potentials for an urbanization mitigation wedge. *Proceedings of the*

National Academy of Sciences, *112*(20), 6283–6288. https://doi.org/10.1073/pnas.1315545112

Danabasoglu, G., Lamarque, J.-F., Bacmeister, J., Bailey, D. A., DuVivier, A. K., Edwards, J., et al. (2020). The Community Earth System Model Version 2 (CESM2). *Journal of Advances in Modeling Earth Systems*, *12*(2), e2019MS001916. https://doi.org/10.1029/2019MS001916

Demuzere, M., De Ridder, K., & Van Lipzig, N. P. M. (2008). Modeling the energy balance in Marseille: Sensitivity to roughness length parameterizations and thermal admittance. *JOURNAL OF GEOPHYSICAL RESEARCH-ATMOSPHERES*, *113*(D16). https://doi.org/10.1029/2007JD009113

Demuzere, M, Harshan, S., Jarvi, L., Roth, M., Grimmond, C., Masson, V., et al. (2017). Impact of urban canopy models and external parameters on the modelled urban energy balance in a tropical city. *QUARTERLY JOURNAL OF THE ROYAL METEOROLOGICAL SOCIETY*, *143*(704), 1581–1596. https://doi.org/10.1002/qj.3028

Demuzere, Matthias, Oleson, K., Coutts, A. M., Pigeon, G., & van Lipzig, N. P. M. (2013). Simulating the surface energy balance over two contrasting urban environments using the Community Land Model Urban. *INTERNATIONAL JOURNAL OF CLIMATOLOGY*, *33*(15), 3182–3205. https://doi.org/10.1002/joc.3656

Eyring, V., Gleckler, P. J., Heinze, C., Stouffer, R. J., Taylor, K. E., Balaji, V., et al. (2016). Towards improved and more routine Earth system model evaluation in CMIP. *Earth System Dynamics*, *7*(4), 813–830. https://doi.org/10.5194/esd-7-813-2016

761 Fischer, E. M., Oleson, K. W., & Lawrence, D. M. (2012). Contrasting urban and rural heat
762 stress responses to climate change. *GEOPHYSICAL RESEARCH LETTERS*, *39*.
763 https://doi.org/10.1029/2011GL050576
764 Fischer, E. M., Sippel, S., & Knutti, R. (2021). Increasing probability of record-shattering
765 climate extremes. *Nature Climate Change*, *11*(8), 689–695.
766 https://doi.org/10.1038/s41558-021-01092-9
767 Fitria, R., Kim, D., Baik, J., & Choi, M. (2019). Impact of Biophysical Mechanisms on Urban
768 Heat Island Associated with Climate Variation and Urban Morphology. *SCIENTIFIC*
769 *REPORTS*, *9*. https://doi.org/10.1038/s41598-019-55847-8
770 Flanner, M. G. (2009). Integrating anthropogenic heat flux with global climate models.
771 *Geophysical Research Letters*, *36*(2). https://doi.org/10.1029/2008GL036465
772 Gao, J., & O'Neill, B. C. (2020). Mapping global urban land for the 21st century with data-
773 driven simulations and Shared Socioeconomic Pathways. *Nature Communications*, *11*(1),
774 2302. https://doi.org/10.1038/s41467-020-15788-7
775 Gray, L. C., Zhao, L., & Stillwell, A. S. (2023). Impacts of climate change on global total and
776 urban runoff. *Journal of Hydrology*, *620*, 129352.
777 https://doi.org/10.1016/j.jhydrol.2023.129352
778 Gregory, P. J., Ingram, J. S. I., & Brklacich, M. (2005). Climate change and food security.
779 *Philosophical Transactions of the Royal Society B: Biological Sciences*, *360*(1463),
780 2139–2148. https://doi.org/10.1098/rstb.2005.1745
781 Grimm, N. B., Faeth, S. H., Golubiewski, N. E., Redman, C. L., Wu, J., Bai, X., & Briggs, J. M.
782 (2008). Global change and the ecology of cities. *SCIENCE*, *319*(5864), 756–760.
783 https://doi.org/10.1126/science.1150195

He, C., Liu, Z., Wu, J., Pan, X., Fang, Z., Li, J., & Bryan, B. A. (2021). Future global urban water scarcity and potential solutions. *Nature Communications*, *12*(1), 4667. https://doi.org/10.1038/s41467-021-25026-3

Hertwig, D., Ng, M., Grimmond, S., Vidale, P. L., & McGuire, P. C. (2021). High-resolution global climate simulations: Representation of cities. *International Journal of Climatology*, *41*(5), 3266–3285. https://doi.org/10.1002/joc.7018

Horton, R. M., Mankin, J. S., Lesk, C., Coffel, E., & Raymond, C. (2016). A Review of Recent Advances in Research on Extreme Heat Events. *Current Climate Change Reports*, *2*(4), 242–259. https://doi.org/10.1007/s40641-016-0042-x

Hsu, A., Sheriff, G., Chakraborty, T., & Manya, D. (2021). Disproportionate exposure to urban heat island intensity across major US cities. *Nature Communications*, *12*(1), 2721. https://doi.org/10.1038/s41467-021-22799-5

Huang, K., Lee, X., Stone Jr., B., Knievel, J., Bell, M. L., & Seto, K. C. (2021). Persistent Increases in Nighttime Heat Stress From Urban Expansion Despite Heat Island Mitigation. *Journal of Geophysical Research: Atmospheres*, *126*(4), e2020JD033831. https://doi.org/10.1029/2020JD033831

Hurtt, G. C., Chini, L., Sahajpal, R., Frolking, S., Bodirsky, B. L., Calvin, K., et al. (2020). Harmonization of global land use change and management for the period 850–2100 (LUH2) for CMIP6. *Geoscientific Model Development*, *13*(11), 5425–5464. https://doi.org/10.5194/gmd-13-5425-2020

IPCC. (2014). *Climate Change 2014: Mitigation of Climate Change. Contribution of Working Group III to the Fifth Assessment*. Retrieved from https://www.ipcc.ch/report/ar5/wg3/

IPCC. (2021). *Climate Change 2021: The Physical Science Basis. Contribution of Working Group I to the Sixth Assessment Report of the Intergovernmental Panel on Climate Change* (Vol. In Press). Cambridge, United Kingdom and New York, NY, USA: Cambridge University Press. https://doi.org/10.1017/9781009157896

IPCC. (2022). Climate Change 2022: Impacts, Adaptation and Vulnerability. Cambridge, UK and New York, USA: Cambridge University Press.

Jackson, T. L., Feddema, J. J., Oleson, K. W., Bonan, G. B., & Bauer, J. T. (2010). Parameterization of Urban Characteristics for Global Climate Modeling. *Annals of the Association of American Geographers*, *100*(4), 848–865. https://doi.org/10.1080/00045608.2010.497328

Karsisto, P., Fortelius, C., Demuzere, M., Grimmond, C. S. B., Oleson, K. W., Kouznetsov, R., et al. (2016). Seasonal surface urban energy balance and wintertime stability simulated using three land-surface models in the high-latitude city Helsinki. *QUARTERLY JOURNAL OF THE ROYAL METEOROLOGICAL SOCIETY*, *142*(694, A), 401–417. https://doi.org/10.1002/qj.2659

Kaur, R., & Pandey, P. (2021). Air Pollution, Climate Change, and Human Health in Indian Cities: A Brief Review. *Frontiers in Sustainable Cities*, *3*. Retrieved from https://www.frontiersin.org/articles/10.3389/frsc.2021.705131

Knutti, R., & Sedlacek, J. (2013). Robustness and uncertainties in the new CMIP5 climate model projections. *NATURE CLIMATE CHANGE*, *3*(4), 369–373. https://doi.org/10.1038/NCLIMATE1716

827 Krayenhoff, E. S., Moustaoui, M., Broadbent, A., Gupta, V., & Georgescu, M. (2018). Diurnal
828 interaction between urban expansion, climate change and adaptation in US cities. *Nature*
829 *Climate Change*, *8*(12), 1097–1103. https://doi.org/10.1038/s41558-018-0320-9
830 Krayenhoff, E. S., Broadbent, A. M., Zhao, L., Georgescu, M., Middel, A., Voogt, J. A., et al.
831 (2021). Cooling hot cities: a systematic and critical review of the numerical modelling
832 literature. *Environmental Research Letters*, *16*(5), 053007. https://doi.org/10.1088/1748-
833 9326/abdcf1
834 Lai, Y., & Dzombak, D. A. (2021). Assessing the Effect of Changing Ambient Air Temperature
835 on Water Temperature and Quality in Drinking Water Distribution Systems. *Water*,
836 *13*(14), 1916. https://doi.org/10.3390/w13141916
837 Lai, Y., Lopez-Cantu, T., Dzombak, D. A., & Samaras, C. (2022). Framing the Use of Climate
838 Model Projections in Infrastructure Engineering: Practices, Uncertainties, and
839 Recommendations. *Journal of Infrastructure Systems*, *28*(3), 04022020.
840 https://doi.org/10.1061/(ASCE)IS.1943-555X.0000685
841 Lawrence, D. M., Fisher, R. A., Koven, C. D., Oleson, K. W., Swenson, S. C., Bonan, G., et al.
842 (2019). The Community Land Model Version 5: Description of New Features,
843 Benchmarking, and Impact of Forcing Uncertainty. *Journal of Advances in Modeling*
844 *Earth Systems*, *11*(12), 4245–4287. https://doi.org/10.1029/2018MS001583
845 Li, D., & Bou-Zeid, E. (2013). Synergistic Interactions between Urban Heat Islands and Heat
846 Waves: The Impact in Cities Is Larger than the Sum of Its Parts. *Journal of Applied*
847 *Meteorology and Climatology*, *52*(9), 2051–2064. https://doi.org/10.1175/JAMC-D-13-
848 02.1

Li, D., Malyshev, S., & Shevliakova, E. (2016a). Exploring historical and future urban climate in the Earth System Modeling framework: 1. Model development and evaluation. *Journal of Advances in Modeling Earth Systems*, *8*(2), 917–935. https://doi.org/10.1002/2015MS000578

Li, D., Malyshev, S., & Shevliakova, E. (2016b). Exploring historical and future urban climate in the Earth System Modeling framework: 2. Impact of urban land use over the Continental United States. *Journal of Advances in Modeling Earth Systems*, *8*(2), 936–953. https://doi.org/10.1002/2015MS000579

Li, J., Chen, Y. D., Gan, T. Y., & Lau, N.-C. (2018). Elevated increases in human-perceived temperature under climate warming. *NATURE CLIMATE CHANGE*, *8*(1), 43+. https://doi.org/10.1038/s41558-017-0036-2

Li, Y., Ren, T., Kinney, P. L., Joyner, A., & Zhang, W. (2018). Projecting future climate change impacts on heat-related mortality in large urban areas in China. *Environmental Research*, *163*, 171–185. https://doi.org/10.1016/j.envres.2018.01.047

Liu, W., You, H., & Dou, J. (2009). Urban-rural humidity and temperature differences in the Beijing area. *Theoretical and Applied Climatology*, *96*(3), 201–207. https://doi.org/10.1007/s00704-008-0024-6

Liu, Z., Yang, Y., He, C., & Tu, M. (2019). Climate change will constrain the rapid urban expansion in drylands: A scenario analysis with the zoned Land Use Scenario Dynamics-urban model. *Science of The Total Environment*, *651*, 2772–2786. https://doi.org/10.1016/j.scitotenv.2018.10.177

Luo, M., & Lau, N.-C. (2018). Increasing Heat Stress in Urban Areas of Eastern China: Acceleration by Urbanization. *Geophysical Research Letters*, *45*(23), 13,060-13,069. https://doi.org/10.1029/2018GL080306

Luo, M., & Lau, N.-C. (2019). Urban Expansion and Drying Climate in an Urban Agglomeration of East China. *Geophysical Research Letters*, *46*(12), 6868–6877. https://doi.org/10.1029/2019GL082736

Manoli, G., Fatichi, S., Schläpfer, M., Yu, K., Crowther, T. W., Meili, N., et al. (2019). Magnitude of urban heat islands largely explained by climate and population. *Nature*, *573*(7772), 55–60. https://doi.org/10.1038/s41586-019-1512-9

Masson, V. (2006). Urban surface modeling and the meso-scale impact of cities. *Theoretical and Applied Climatology*, *84*(1–3), 35–45. https://doi.org/10.1007/s00704-005-0142-3

Meehl, G. A., & Tebaldi, C. (2004). More Intense, More Frequent, and Longer Lasting Heat Waves in the 21st Century. *Science*, *305*(5686), 994–997. https://doi.org/10.1126/science.1098704

Meili, N., Paschalis, A., Manoli, G., & Fatichi, S. (2022). Diurnal and seasonal patterns of global urban dry islands. *Environmental Research Letters*, *17*(5), 054044. https://doi.org/10.1088/1748-9326/ac68f8

Mora, C., Dousset, B., Caldwell, I. R., Powell, F. E., Geronimo, R. C., Bielecki, C. R., et al. (2017). Global risk of deadly heat. *Nature Climate Change*, *7*(7), 501–506. https://doi.org/10.1038/nclimate3322

Niyogi, D., Pyle, P., Lei, M., Arya, S. P., Kishtawal, C. M., Shepherd, M., et al. (2011). Urban Modification of Thunderstorms: An Observational Storm Climatology and Model Case

892 Study for the Indianapolis Urban Region. *JOURNAL OF APPLIED METEOROLOGY*
893 *AND CLIMATOLOGY*, *50*(5), 1129–1144. https://doi.org/10.1175/2010JAMC1836.1
894 Oleson, K. (2012). Contrasts between Urban and Rural Climate in CCSM4 CMIP5 Climate
895 Change Scenarios. *JOURNAL OF CLIMATE*, *25*(5), 1390–1412.
896 https://doi.org/10.1175/JCLI-D-11-00098.1
897 Oleson, K. W., & Feddema, J. (2020). Parameterization and Surface Data Improvements and
898 New Capabilities for the Community Land Model Urban (CLMU). *Journal of Advances*
899 *in Modeling Earth Systems*, *12*(2), e2018MS001586.
900 https://doi.org/10.1029/2018MS001586
901 Oleson, K. W., Bonan, G. B., Feddema, J., Vertenstein, M., & Grimmond, C. S. B. (2008). An
902 urban parameterization for a global climate model. Part I: Formulation and evaluation for
903 two cities. *JOURNAL OF APPLIED METEOROLOGY AND CLIMATOLOGY*, *47*(4),
904 1038–1060. https://doi.org/10.1175/2007JAMC1597.1
905 Oleson, K. W., Bonan, G. B., Feddema, J., & Vertenstein, M. (2008). An urban parameterization
906 for a global climate model. Part II: Sensitivity to input parameters and the simulated
907 urban heat island in offline Simulations. *JOURNAL OF APPLIED METEOROLOGY*
908 *AND CLIMATOLOGY*, *47*(4), 1061–1076. https://doi.org/10.1175/2007JAMC1598.1
909 Oleson, W., Bonan, B., Feddema, J., Vertenstein, M., & Kluzek, E. (2010). Technical
910 Description of an Urban Parameterization for the Community Land Model (CLMU).
911 https://doi.org/10.5065/D6K35RM9
912 O'Neill, B. C., Tebaldi, C., van Vuuren, D. P., Eyring, V., Friedlingstein, P., Hurtt, G., et al.
913 (2016). The Scenario Model Intercomparison Project (ScenarioMIP) for CMIP6.

914 *Geoscientific Model Development*, *9*(9), 3461–3482. https://doi.org/10.5194/gmd-9-3461-
915 2016
916 Pal, J. S., & Eltahir, E. A. B. (2016). Future temperature in southwest Asia projected to exceed a
917 threshold for human adaptability. *Nature Climate Change*, *6*(2), 197–200.
918 https://doi.org/10.1038/nclimate2833
919 Patz, J. A., Campbell-Lendrum, D., Holloway, T., & Foley, J. A. (2005). Impact of regional
920 climate change on human health. *Nature*, *438*(7066), 310–317.
921 https://doi.org/10.1038/nature04188
922 Qian, Y., Chakraborty, T. C., Li, J., Li, D., He, C., Sarangi, C., et al. (2022). Urbanization Impact
923 on Regional Climate and Extreme Weather: Current Understanding, Uncertainties, and
924 Future Research Directions. *Advances in Atmospheric Sciences*, *39*(6), 819–860.
925 https://doi.org/10.1007/s00376-021-1371-9
926 Salami, R. O., Meding, J. K. von, & Giggins, H. (2017). Vulnerability of human settlements to
927 flood risk in the core area of Ibadan metropolis, Nigeria. *Jàmbá: Journal of Disaster Risk*
928 *Studies*, *9*(1), 14. https://doi.org/10.4102/jamba.v9i1.371
929 Seto, K. C., Dhakal, S., Bigio, A., Blanco, H., Delgado, G. C., Dewar, D., et al. (2014). Human
930 Settlements, Infrastructure, and Spatial Planning. In *Climate Change 2014: Mitigation of*
931 *Climate Change. Contribution of Working Group III to the Fifth Assessment Report of the*
932 *Intergovernmental Panel on Climate Change*.
933 Seto, K. C., Golden, J. S., Alberti, M., & Turner, B. L. (2017). Sustainability in an urbanizing
934 planet. *Proceedings of the National Academy of Sciences*, *114*(34), 8935–8938.
935 https://doi.org/10.1073/pnas.1606037114

936 Taylor, K. E., Stouffer, R. J., & Meehl, G. A. (2012). An Overview of CMIP5 and the
937 Experiment Design. *Bulletin of the American Meteorological Society*, *93*(4), 485–498.
938 https://doi.org/10.1175/BAMS-D-11-00094.1
939 Tuholske, C., Caylor, K., Funk, C., Verdin, A., Sweeney, S., Grace, K., et al. (2021). Global
940 urban population exposure to extreme heat. *Proceedings of the National Academy of*
941 *Sciences*, *118*(41), e2024792118. https://doi.org/10.1073/pnas.2024792118
942 UNDESA. (2018). *World urbanization prospects: the 2018 revision*. New York: United Nations.
943 Vermeulen, S. J., Aggarwal, P. K., Ainslie, A., Angelone, C., Campbell, B. M., Challinor, A. J.,
944 et al. (2012). Options for support to agriculture and food security under climate change.
945 *Environmental Science & Policy*, *15*(1), 136–144.
946 https://doi.org/10.1016/j.envsci.2011.09.003
947 William Solecki, Karen C. Seto, & Peter J. Marcotullio. (2013). It's Time for an Urbanization
948 Science. In *Environment: Science and Policy for Sustainable Development* (Vol. 55–1, pp.
949 12–17). Retrieved from
950 https://www.tandfonline.com/doi/abs/10.1080/00139157.2013.748387
951 Yang, B., Yang, X., Leung, L. R., Zhong, S., Qian, Y., Zhao, C., et al. (2019). Modeling the
952 Impacts of Urbanization on Summer Thermal Comfort: The Role of Urban Land Use and
953 Anthropogenic Heat. *JOURNAL OF GEOPHYSICAL RESEARCH-ATMOSPHERES*,
954 *124*(13), 6681–6697. https://doi.org/10.1029/2018JD029829
955 Yang, J., Zhao, L., & Oleson, K. (2023). Large humidity effects on urban heat exposure and
956 cooling challenges under climate change. *Environmental Research Letters*, *18*(4), 044024.
957 https://doi.org/10.1088/1748-9326/acc475

Ye, B., Jiang, J., Liu, J., Zheng, Y., & Zhou, N. (2021). Research on quantitative assessment of climate change risk at an urban scale: Review of recent progress and outlook of future direction. *Renewable and Sustainable Energy Reviews*, *135*, 110415. https://doi.org/10.1016/j.rser.2020.110415

Zhao, L. (2018). Urban growth and climate adaptation. *Nature Climate Change*, *8*(12), 1034–1034. https://doi.org/10.1038/s41558-018-0348-x

Zhao, L., Lee, X., Smith, R. B., & Oleson, K. (2014). Strong contributions of local background climate to urban heat islands. *Nature*, *511*(7508), 216–219. https://doi.org/10.1038/nature13462

Zhao, L., Lee, X., & Schultz, N. M. (2017a). A wedge strategy for mitigation of urban warming in future climate scenarios. *Atmospheric Chemistry and Physics*, *17*(14), 9067–9080. https://doi.org/10.5194/acp-17-9067-2017

Zhao, L., Lee, X., & Schultz, N. M. (2017b). A wedge strategy for mitigation of urban warming in future climate scenarios. *ATMOSPHERIC CHEMISTRY AND PHYSICS*, *17*(14), 9067–9080. https://doi.org/10.5194/acp-17-9067-2017

Zhao, L., Oppenheimer, M., Zhu, Q., Baldwin, J. W., Ebi, K. L., Bou-Zeid, E., et al. (2018). Interactions between urban heat islands and heat waves. *Environmental Research Letters*, *13*(3), 034003. https://doi.org/10.1088/1748-9326/aa9f73

Zhao, L., Oleson, K., Bou-Zeid, E., Krayenhoff, E. S., Bray, A., Zhu, Q., et al. (2021a). Global multi-model projections of local urban climates. *Nature Climate Change*, *11*(2), 152–157. https://doi.org/10.1038/s41558-020-00958-8

Zhao, L., Oleson, K., Bou-Zeid, E., Krayenhoff, E. S., Bray, A., Zhu, Q., et al. (2021b). Global multi-model projections of local urban climates. *Nature Climate Change*, *11*(2), 152–157. https://doi.org/10.1038/s41558-020-00958-8

Zheng, Z., Zhao, L., & Oleson, K. W. (2021). Large model structural uncertainty in global projections of urban heat waves. *NATURE COMMUNICATIONS*, *12*(1), 3736.

Zscheischler, J., Westra, S., van den Hurk, B. J. J. M., Seneviratne, S. I., Ward, P. J., Pitman, A., et al. (2018). Future climate risk from compound events. *Nature Climate Change*, *8*(6), 469–477. https://doi.org/10.1038/s41558-018-0156-3